Nanoscale

Accepted Manuscript

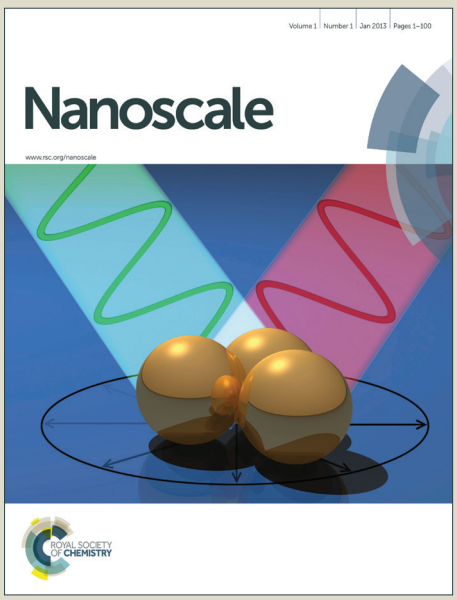

ROYAL SOCIETY OF CHEMISTRY

www.rsc.org/nanoscale

Cite this: DOI: 10.1039/c0xx00000x

www.rsc.org/xxxxxx

ARTICLE TYPE

A novel three-dimensional spherical $CuBi_2O_4$ nanocolumn arrays with persulfate and peroxymonosulfate activation functionalities for 1H-benzotriazole removal

Wen-Da Oh[a, b], Shun-Kuang Lua[a, c], Zhili Dong[a, c] and Teik-Thye Lim[a, b]*

Received (in XXX, XXX) Xth XXXXXXXXX 20XX, Accepted Xth XXXXXXXXX 20XX
DOI: 10.1039/b000000x

Abstract: A novel $CuBi_2O_4$ consisting of self-assembled spherical nanocolumn arrays (CuB-H) was synthesized via a facile hydrothermal method. It was further modified by controlling the Cu:Bi ratio during synthesis to become an efficient bi-functional catalyst (CuB-2.5) activate persulfate (PS) and peroxymonosulfate (PMS) for 1H-benzotriazole (BTZ) removal. Characterization of CuB-2.5 using XRD, FESEM, FTIR, BET and XPS revealed that it was morphologically similar to CuB-H and the molecular formula, as determined from the XRD results, was $Cu_{1.2}Bi_{1.6}O_{3.6}$ with 2.4% w/w of CuO. The CuB-2.5 catalyst exhibited superior performance for BTZ removal via PS and PMS activations over the Cu^{2+} (aq), CuO, $CuBi_2O_4$ (CuB-M, microsphere) and CuB-H. The performance of CuB-2.5 was investigated at different initial PS/PMS dosages, initial catalyst loadings and initial BTZ concentrations. Interestingly, it was found that the inter- and intra-molecular hydrogen bonding plays a prominent role in the BTZ removal mechanism in both the PS and PMS systems. Meanwhile, PMS is relatively easier to be activated leading to a faster BTZ removal rate over the PS system. The intermediate products of BTZ degradation produced from the PS and PMS systems were similar indicating the similar degradation pathway. The catalyst could still retain its morphology and can be reused multiple times.

Keywords: Persulfate activation; Peroxymonosulfate activation; Sulfate radical; Hydroxyl radical; Benzotriazole.

1. Introduction

Advanced oxidation processes (AOPs) employing peroxymonosulfate (PMS) and persulfate (PS) activations to generate reactive oxidizing species for abating recalcitrant organics in water are gaining attention as efficient treatment methods [1]. PMS can be commercially purchased in the form of triple salt ($2KHSO_5.KHSO_4.K_2SO_4$, Oxone®) and it has a lower oxidation potential than PS (E_o = 1.82 V vs E_o = 2.01 V) [2]. However, PMS is relatively easier to be activated to produce sulfate radicals ($SO_4^{\bullet-}$) compared with PS [3]. An effective strategy for *in situ* activation of PS and PMS is by redox reaction with transition metal. In PMS activation, redox reaction with transition metal species (e.g.: Co^{2+}, Fe^{3+}, Cu^{2+} etc.) can produce reactive sulfate and PMS ($SO_5^{\bullet-}$) radicals (Eqs. (1) and (2))[4]. Similarly, redox reaction between PS and transition metal (Fe^0, Fe^{2+}) can also produce $SO_4^{\bullet-}$. However, PS reaction generating $SO_4^{\bullet-}$ is a one way reaction and the activator is consumed during the treatment process (Eq. (3)).

Transition metal (Tm) activation of PMS

$$HSO_5^- + Tm^{n+} \rightarrow Tm^{(n+1)+} + SO_4^{\bullet-} + OH^- \quad (1)$$

$$HSO_5^- + Tm^{(n+1)+} \rightarrow Tm^{n+} + SO_5^{\bullet-} + H^+ \quad (2)$$

Transition metal (Tm) activation of PS

$$S_2O_8^- + Tm^{n+} \rightarrow Tm^{(n+1)+} + SO_4^{\bullet-} + SO_4^{2-} \quad (3)$$

In a recent study, Zhang et al. reported that PS can also be activated by Cu catalyst in the heterogeneous system to produce reactive species, albeit not as reactive as $SO_4^{\bullet-}$ [5]. This process does not deplete the activator and can effectively degrade various organic pollutants. The Cu heterogeneous catalyst has also been reported as an efficient catalyst for PMS activation [6, 7]. Since most catalysts for PMS activation are not efficient for PS activation and vice versa, this provides an attractive avenue to develop a catalyst that can activate both PS and PMS efficiently.

1H-benzotriazole (BTZ) is a highly soluble (28 g L^{-1} in water) and polar heterocyclic compound with a benzo-fused azole moiety. BTZ is produced in large quantity for applications in the automotive industry (antifreeze agent), aviation industry (de-icing fluid), as corrosion inhibitor, as part of formulation in fluids for brakes and metal-cutting and industrial cooling systems [8]. BTZ is biologically active and has both estrogenic and anti-estrogenic effects on aquatic life [9, 10]. Due to its ubiquitous use and recalcitrant nature, BTZ has been detected in the surface water

[11, 12]. BTZ is toxic and resistant to biodegradation and therefore, current conventional wastewater treatment plants (e.g.: activated sludge) have difficulty removing BTZ from water [13]. Previously, several studies have been conducted to evaluate BTZ removal efficiency from water using sorption, photoelectro-fenton like process, ozone treatment, and photocatalysis [13-16]. Although sorption process is effective, the spent sorbent creates a secondary waste problem. Photoelectro-fenton like process, ozone treatment and photocatalysis rely on the generation of hydroxyl radicals ($HO^{\bullet}$) for effective BTZ degradation. Comparing $HO^{\bullet}$ with $SO_4^{\bullet-}$, $SO_4^{\bullet-}$ is more stable, selective and has a relatively longer lifetime (10^{-3} vs. 30-40 µs) thus allowing better utilization of the generated radicals [17, 18]. In addition, $SO_4^{\bullet-}$ has a relatively stronger oxidizing power than $HO^{\bullet}$ at elevated pH [19]. To date, reports on the treatment of BTZ via generation of reactive radicals by heterogeneous transition metal activation of PS and PMS are lacking.

Herein, a facile hydrothermal synthesis method was employed to prepare $CuBi_2O_4$ catalyst with novel three-dimensional (3D) spherical nanocolumn arrays morphology. The catalyst was further modified to become a bi-functional catalyst which can activate both PS and PMS efficiently for BTZ removal. The mechanisms of PS/PMS activation by the bi-functional $CuBi_2O_4$ catalyst were proposed. The effects of several operational parameters, namely initial BTZ concentration, catalyst loading and initial PS/PMS dosage were investigated. Additionally, the influence of chloride ions on BTZ degradation via PMS/PS activation was evaluated. The intermediate products of BTZ degradation via PS/PMS activation were also studied.

2. Experimental

2.1 Chemicals

The chemicals used in this study were of analytical grade without further purification. The chemicals were $Cu(NO_3)_2.3H_2O$ (Qrëc™), $Bi(NO_3)_3.5H_2O$ (Alfa Aesar), HNO_3 (Merck), NaOH (Alfa Aesar), PMS in the form of Oxone® (2KHSO5.KHSO4.K2SO4, Alfa Aesar), $K_2S_2O_8$ (Sigma-Aldrich), methanol (Merck), NaCl (Qrëc™), KI (Fisons) and 1H-benzotriazole (BTZ, Alfa Aesar). The Milli-Q ultrapure water with resistivity of 18.2 MΩ cm was used in all the experiments.

2.2 Synthesis

The catalysts were synthesized by a facile one-pot hydrothermal synthesis without using any template or surfactant. In a typical preparation procedure, 2 mmol of $Cu(NO_3)_2.3H_2O$ and 4 mmol $Bi(NO_3)_3.5H_2O$ were fully dissolved in 50 mL of 0.5 M HNO_3 while under stirring. Then, 25 mL of 2 M NaOH was slowly added into the solution while under stirring. The final pH was recorded to be pH 14. After rapid magnetic stirring for 1 h, the solution mixture was sealed in a 125-mL Teflon-lined stainless steel autoclave and heated in an oven at 200 °C under autogeneous pressure for 12 h. The resultant brownish-black product was washed with DI water and dried in an oven at 60 °C for at least 4 h. The effects of different synthesis conditions were studied by varying the synthesis temperature (140 – 200 °C), Cu:Bi mol ratio of 1:2 – 3:2 and NaOH molarity (1-6 M). For comparison, the CuO catalyst was also synthesized using the above-mentioned hydrothermal protocols except without the addition of $Bi(NO_3)_3.5H_2O$.

2.3 Characterization techniques

The mineralogy and crystal structures of the as-prepared catalysts were analyzed using a X-ray diffractometer (Bruker D8 Advance XRD) operating on a high intensity Cu-Kα X-ray source at 40 kV and 40 mA. The catalyst samples were scanned from 10-90° at a scan rate of 0.05°/s. The morphological detail of the catalysts was examined using a field emission scanning electron microscope (FESEM, JEOL-7600F). The Brunauer-Emmet-Teller (BET) specific surface area was determined by analyzing the N_2 adsorption-desorption isotherm at 77 K (Quantachrome Autosorb-1 Analyzer). The X-ray photoelectron spectroscopy (XPS) measurement was conducted using a Phoibos 100 spectrometer equipped with a monochromatic Mg X-ray source (SPECS, Germany). The XPS data was calibrated against the adventitious C 1s peak at the binding energy of 284.8 eV. The Fourier transform infrared spectroscopy (FTIR, Perkin Elmer) was employed to investigate the surface functional group of the catalyst.

2.4 Performance study

The performance of the as-prepared catalysts was evaluated for the treatment of BTZ in a batch system at ambient temperature. In a typical experimental procedure, 100 mL of solution containing 2.5 mg L^{-1} of BTZ was added into a 250-mL reactive vessel. Then, a known amount of PS/ PMS was dissolved into the solution in the reaction vessel under rapid stirring. The pH was then immediately adjusted to pH 7 using 1 M NaOH. Under rapid stirring, the catalytic BTZ degradation study was initiated (t = 0 min) once 0.5 g L^{-1} of the catalyst was introduced into the reaction vessel. Sampling of the solution was conducted at various time intervals by drawing 1-mL of the aliquot from the reaction vessel and filtering using a cellulose acetate filter to determine the BTZ concentration. Methanol was used to quench the reaction. The experiment was repeated by using different catalysts (i.e. selected catalysts prepared with different hydrothermal conditions). For PS system, the experiment was repeated by varying the initial PS dosage (0.1-0.8 g L^{-1}) and catalyst dosage (0.5-2.0 g L^{-1}). For PMS system, the experiment was also repeated by varying the initial PMS dosage (0.05-0.20 g L^{-1}) and BTZ concentration (2.5-10.0 g L^{-1}). Control experiments were carried out by repeating the above-mentioned protocols but (i) without catalyst, (ii) without oxidant, and (iii) without catalyst and oxidant. All the experiments were conducted in duplicate.

The total organic carbon (TOC), Cu leaching, degradation products and PMS/PS consumption were determined at the end of the reaction time (t_{PS} = 90 min, t_{PMS} = 10 min) at the following experimental conditions : for PS, initial pH = 7, initial PS dosage = 0.8 g L^{-1}, initial catalyst loading = 2.0 g L^{-1}; for PMS, initial pH = 7, initial PMS dosage = 0.2 g L^{-1}, initial catalyst dosage = 0.5 g L^{-1}). The TOC and Cu leaching experiment at the end of the reaction time was conducted without employing methanol as the quencher For TOC experiment, the analysis was carried out immediately after the end of the reaction. The Cl^- can act as a radical scavenger for $SO_4^{\bullet-}$ with second-order rate constant of 2.8 x 10^{-8} M^{-1} s^{-1} [20]. Therefore, it is an important water matrix species that could interfere and exert detrimental effect to the BTZ degradation [21, 22]. The effects of Cl^- on BTZ degradation

in the PS and PMS systems were investigated by conducting the BTZ oxidation reaction in the presence of Cl^- at various concentrations (0-500 mg L^{-1}). The steady-state [$SO_4^{\bullet-}$] concentration for the PMS system was estimated from the rate of $SO_4^{\bullet-}$ oxidation of benzene by conducting the catalytic experiment with benzene instead of BTZ. The reusability of the catalyst was also evaluated up to three cycles for both PS and PMS systems to determine the stability of the catalyst.

2.5 Analytical methods

The BTZ concentration was determined using a high performance liquid chromatography (HPLC, Perkin Elmer) equipped with a UV detector at λ_{max} = 256 nm. The mobile phase consisted of methanol to ultrapure water ratio of 1:1 at the flow rate of 1 mL min^{-1} while the column used was a reverse phase HPLC column (Hypersil Gold). The TOC measurement was conducted by using a TOC analyzer (Shimadzu TOC analyzer). The PS/PMS concentration was determined by using the spectrophotometric method at λ_{max} = 352 nm as described by Oh et al. [17]. The Cu concentration was determined by using an inductively-coupled plasma-optical emission spectrometer (ICP-OES, Perkin Elmer Optima 2000DV).

The BTZ degradation products after degradation were identified using a Shimadzu LC-MS 8030 equipped with electrospray ionization (ESI) source in positive and negative modes. The N_2 gas was used as the nebulizing and drying gas at the flow rates of 3 and 15 L min^{-1}, respectively. The samples were injection via a flow injection analysis method and the injection volume was 10 µL at the flow rate of 0.2 mL min^{-1}. The mobile phase used was 1:1 ratio of methanol and ultrapure water, both with 0.1% v/v of formic acid. The heat block and DL temperatures were 400 and 250 °C, respectively. The m/z was scanned from 50-400.

3. Results and discussions

3.1 Synthesis and characterization studies

Single phase tetragonal $CuBi_2O_4$ with space group *P4/ncc* was successfully synthesized by a facile one-pot hydrothermal synthesis route. The mechanism of formation of the $CuBi_2O_4$ during the hydrothermal reaction involves (i) the initial formation of $Cu(OH)_2$ and $Bi(OH)_3$, (ii) hydrolysis reaction, and (iii) lattice fusion of CuO and Bi_2O_3 forming $CuBi_2O_4$ nucleus (iv) anisotropic/isotropic growth of $CuBi_2O_4$[23]. Fig. 1 shows the schematic illustration of various synthesis conditions and their corresponding structures while Fig. 2 shows the FESEM micrographs of the $CuBi_2O_4$ prepared under various synthesis conditions. The $CuBi_2O_4$ with near perfect microspherical morphology can be easily formed at T = 140 °C (CuB-M, diameter = 3-5 µm, Fig. 2a). Control of the size of the microsphere can be easily achieved by decreasing or increasing the amount of metal precursors (Fig. S1a and d). Similarly, by increasing the Cu:Bi ratio, reduction of the average microsphere size was also observed (Fig. S1d-f) but resulted in the presence CuO impurity. Higher Cu:Bi ratio favors nucleation of $CuBi_2O_4$ but retards the growth of the nucleus.

By careful control of the reaction temperature and NaOH molarity, the microsphere morphology of the $CuBi_2O_4$ can be tailored to well-defined hierarchical three-dimensional (3-D) self-assembly of $CuBi_2O_4$ nanocolumn arrays (CuB-H, length = 1-1.5 µm, Fig. 2b) with uniform distribution. Unlike the previous studies [23, 24], which employed polyethylene glycol or introduced ethanol as a co-solvent for morphological control, the synthesis in this study was carried out without the use of any template or surfactant. The $CuBi_2O_4$ nanocolumns spontaneously self-assembled under high autogeneous pressure at 200 °C achieving the lowest Gibbs free energy by forming a 3-D spherical nanocolumn arrays connected through non-covalent interactions. An incomplete self-assembled CuB-H in Fig. 2c revealed a hollow core with an inner diameter of 1.5 µm resulted from the directional alignment of individual nanocolumns in an ordered fashion. The remarkable influence of Na^+ as structuring ion was evidenced when the 3-D structure could not be obtained with a NaOH molarity of higher than 2 M. Pure phase $CuBi_2O_4$ could not be formed with a NaOH molarity < 2 M which can be attributed to the deficiency of OH^- to form $CuBi_2O_4$ (pH = 14). Xie et al. also reported the significance of controlling the NaOH molarity to obtain $CuBi_2O_4$ with leaf-like morphology for photocatalysis application [25].

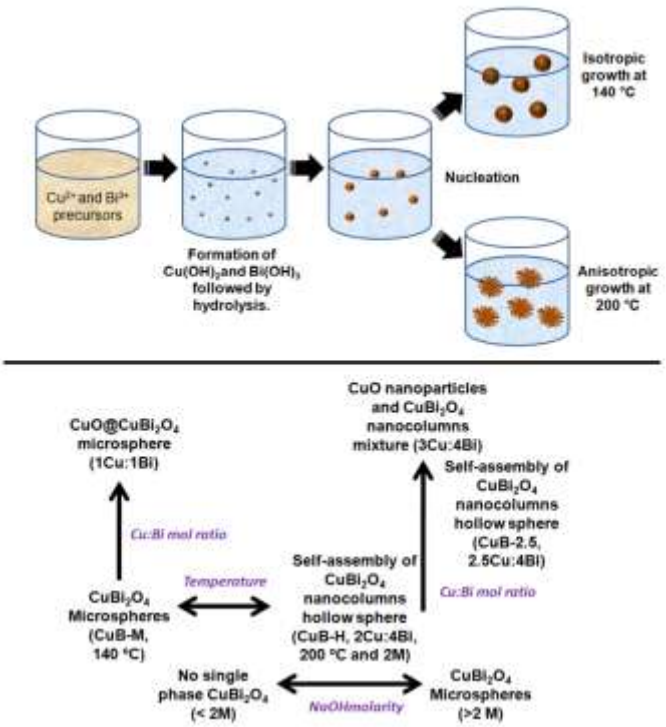

Fig. 1: Schematic illustration of the synthesis conditions and their morphological results.

The Cu(II) transition metal plays an active role in the activation of PS and PMS [6, 26]. Since the main purpose of this paper is to develop an efficient catalyst with PS and PMS activation functionalities, the Cu:Bi ratio during synthesis was further elevated from stoichiometry ratio to 2.5:4 (denoted as CuB-2.5) with the intention to enhance the performance of the catalyst. Interestingly, the 3-D morphology of CuB-H could be retained in CuB-2.5. A small amount of sub-micron particles, most likely CuO (size = 20-30 nm), was anchored on the surface of the $CuBi_2O_4$ nanocolumns (Fig. 2d) forming a composite-like

structure. Further increment of the Cu:Bi ratio to 3:4 led to the destruction of the 3-D microstructure resulting in a mixture of $CuBi_2O_4$ nanocolumns and CuO particles (Fig. S1c). This indicated that the optimum Cu:Bi ratio for retaining the morphology is 2.5 to 4.

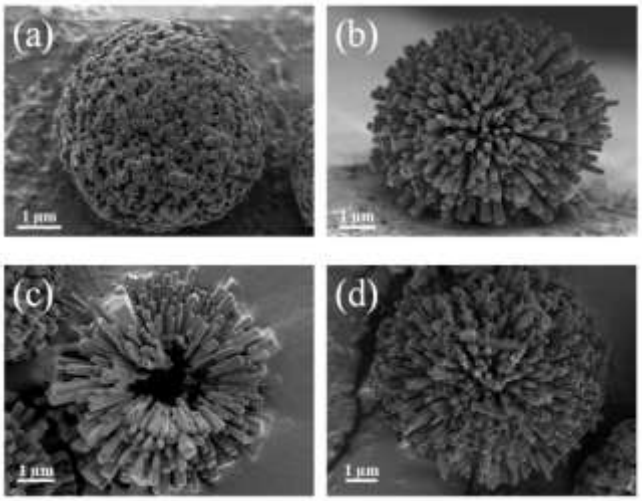

Fig. 2: FESEM images of (a) CuB-M, (b) CuB-H, (c) incomplete self-assembled CuB-H and (d) CuB-2.5.

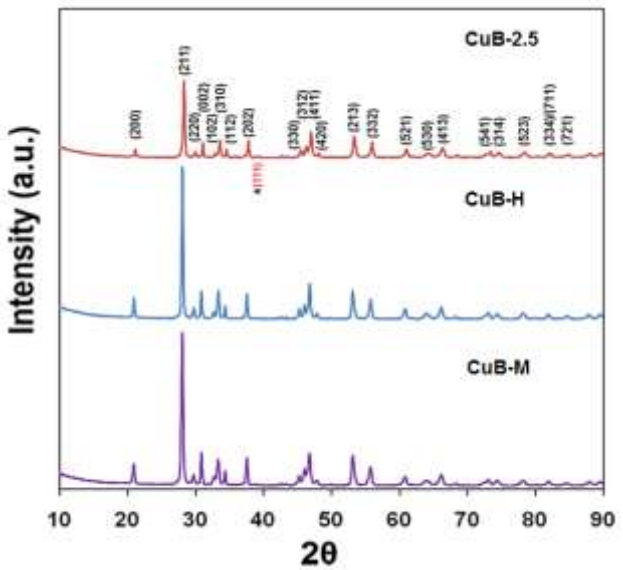

Fig. 3: XRD patterns of CuB-M, CuB-H and CuB-2.5. The (*) indicates the location of the highest intensity (I/I_o) CuO peak.

Fig. 3 shows the XRD patterns of the as-prepared CuB-M, CuB-H and CuB-2.5. All the peaks can be indexed to the pure $CuBi_2O_4$ phase (JCPDS file no. 84-1969). The XRD patterns in Fig. 3 confirm that highly-crystalline single-phase $CuBi_2O_4$ was obtained for CuB-M and CuB-H. Due to the use of non-stoichiometric Cu:Bi ratio and the observation of the sub-micron nanoparticles in CuB-2.5, the XRD pattern of CuB-2.5 is expected to have CuO peaks. However, the XRD diffraction peak with the highest intensity belonging to the CuO at $2\theta = 41°$ (I/I_o = 1), which can be indexed to (111), is relatively weak. This could be attributed to the relatively low amount of CuO (maximum CuO = ca. 3.5% w/w based on 2.5:4 Cu:Bi ratio).

It is also observed that the diffraction peak intensities of CuB-2.5 are generally lower than those obtained for CuB-M and CuB-H which is due to the difference in X-ray scattering factor of Cu and Bi. The lower peak intensities could also be an indicative of a doped material. It is postulated that aside from forming $CuO/CuBi_2O_4$ composite, the additional Cu in CuB-2.5 could also be interstitially doped into the crystal lattice to form non-stoichiometric $Cu_{1+x}Bi_{2-2x}O_{4-2x}$. Further analysis was conducted using rietveld refinement of the XRD patterns indicating that the composition of CuB-2.5 consists of $Cu_{1.2}Bi_{1.6}O_{3.6}$ with 2.4% w/w CuO further supporting the hypothesis. The refinement data for CuB-H and CuB-M showed 100% w/w $CuBi_2O_4$. The CuB-2.5 (18.7 m^2 g^{-1}) exhibited the highest BET specific surface area compared with CuB-H (13.1 m^2 g^{-1}) and CuB-M (4.4 m^2 g^{-1}) allowing higher interacting area for catalysis. Besides improvement in the specific surface area, this strategy increases the overall Cu content from 14% in CuB-H and CuB-M to 20% in CuB-2.5 which is beneficial in enhancing the performance of the catalyst.

Fig. 4 shows the FTIR and XPS spectra of CuB-2.5. The FTIR absorbance bands at 3300 and 1640 cm^{-1} give evidence of the stretching and bending vibrations, respectively, of absorbed water and also the presence of -OH group on the surface of CuB-2.5 [27]. A sharp peak was also observed at 550 cm^{-1} which corresponds to the characteristic peaks of CuO [28]. The XPS spectra of CuB-2.5 in Fig. 4b-c show that the main peaks for Cu 2p, Bi 4f and O1s are at binding energies 933.2, 159.2 and 530.4 eV, respectively, indicating that the oxidation states are Bi^{3+}, Cu^{2+} and O^{2-}[29]. The XPS peaks of Cu from CuO overlap with those from $CuBi_2O_4$. The binding energy of Cu for CuO is 933.7 eV [30] which is very close to 933.2 eV in this study. The oxidation states were in agreement with the theoretical oxidation states of the catalyst.

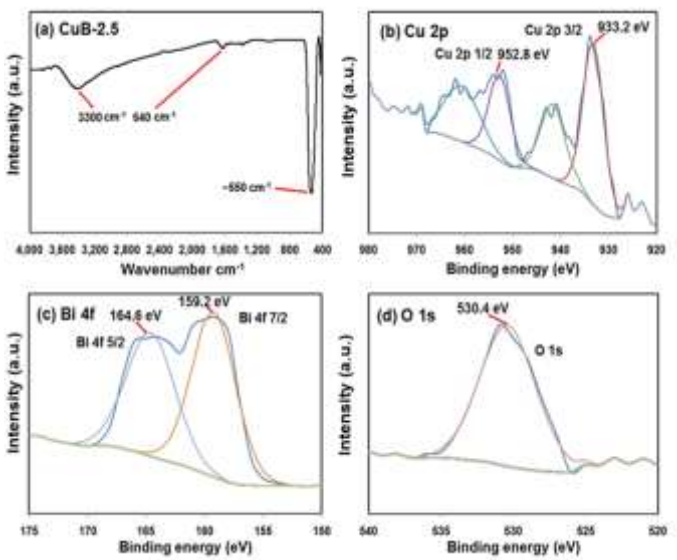

Fig. 4: (a) FTIR spectrum of CuB-2.5, (b) XPS spectra of Cu 2p, (c) XPS spectra of Bi 4f and (d) XPS spectra of O 1s.

3.2 Performance evaluation

3.2.1 PMS and PS activation mechanisms

Three different $CuBi_2O_4$ catalysts, namely CuB-M, CuB-H and

CuB-2.5 were selected for comparison. The catalysts have diverse potentials and advantages for multifunctional application in water treatment. Besides functioning as PS and PMS activators, this material can be tuned to become an efficient photocatalyst. Furthermore, the $CuBi_2O_4$ catalyst has high density and excellent settling velocity. It can be separated by gravity in less than 5 min without the need of advanced separation technique such as the membrane and magnetic separation technologies.

Preliminary study was conducted to evaluate the effect of pH for BTZ degradation (Fig. S2) and pH 7 was selected as an optimum pH due to (i) the slower reaction rate at acidic pH and (ii) to avoid base activation of PS. The catalytic oxidation of BTZ by PS and PMS systems as shown in Fig. 5a and b, respectively, in the preliminary study indicates that all the as-prepared CuB catalysts have PS and PMS activation functionalities. The catalytic oxidation is the main BTZ removal pathway as contributions due to adsorption and direct PS/PMS oxidation on BTZ removal are minimal. In general, the BTZ removal rate and efficiency in the PMS and PS systems follow the order of: Cu^{2+} < CuO < CuB-M < CuB-H < CuB-2.5. This is consistent with the TOC removal efficiencies in the PS and PMS systems in Table 1 which indicate that the extent of mineralization is generally the highest when CuB-2.5 is employed as the catalyst. Judging from the relatively lower catalytic activity of CuO (0.20 g L^{-1}), which is at ~20 times the CuO loading found in CuB-2.5 (0.01 g L^{-1}), the main active species is $Cu_{1.2}Bi_{1.6}O_{3.6}$. A relatively lower TOC removal efficiency was observed for PS/CuB-M and PS/CuB-H systems suggesting that the higher amount of Cu in the CuB-2.5 plays a prominent role in PS activation. Examination of the TOC removal in all the PMS/CuB systems indicated that only 17-18% of TOC was removed within 10 min but by prolonging the reaction time to 90 min, 52-54% of TOC removal efficiency and higher oxidant consumption were achieved. The better performance of CuB-2.5 over CuB-M and CuB-H is attributed to its higher specific surface area and Cu content.

The initial BTZ degradation rate in Fig. 5 was investigated using the pseudo first-order kinetics and the results indicate that the BTZ degradation in the PS/CuB-2.5 system (initial pseudo first-order rate constant for PS system, k_1 = 0.015±0.001 min^{-1}) was ~13 times slower than that in the PMS/CuB-2.5 system (initial pseudo first-order rate constant for PMS system, k_2 = 0.191±0.004 min^{-1}). This is anticipated because the PS activation process involves an outer orbital electron transfer reaction which produces reactive oxidizing species to attack the BTZ molecule. Previous reports has indicated that the generated reactive oxidizing radical was not $O_2^{\bullet-}$ or $SO_4^{\bullet-}$ and has a relatively lower reactivity than that of $SO_4^{\bullet-}$ [5]. It is postulated that the PS molecule can be activated by forming a PS-$CuBi_2O_4$ quasi-complex with specific reactive orientation on the reaction interface. A plausible reactive orientation is presented in Fig. 6. In this orientation, the reactive peroxide bond of PS is exposed making it more susceptible to oxidation and activation reactions compared with the unactivated PS. Based on the molecular structure of BTZ and PS, the intermolecular hydrogen bonding between BTZ and PS is expected to play a key role in drawing the BTZ molecule to close proximity with the reaction interface. Then, the BTZ molecule could serve as an electron donor for subsequent degradation reaction.

$$S_2O_8^{-} + Cu(II)Bi_2O_4 \leftrightarrow S_2O_8^{-}\text{-}Cu(II)Bi_2O_4 \quad (4)$$

$$S_2O_8^{-}\text{-}Cu(II)Bi_2O_4 + BTZ \rightarrow \text{degradation products} \quad (5)$$

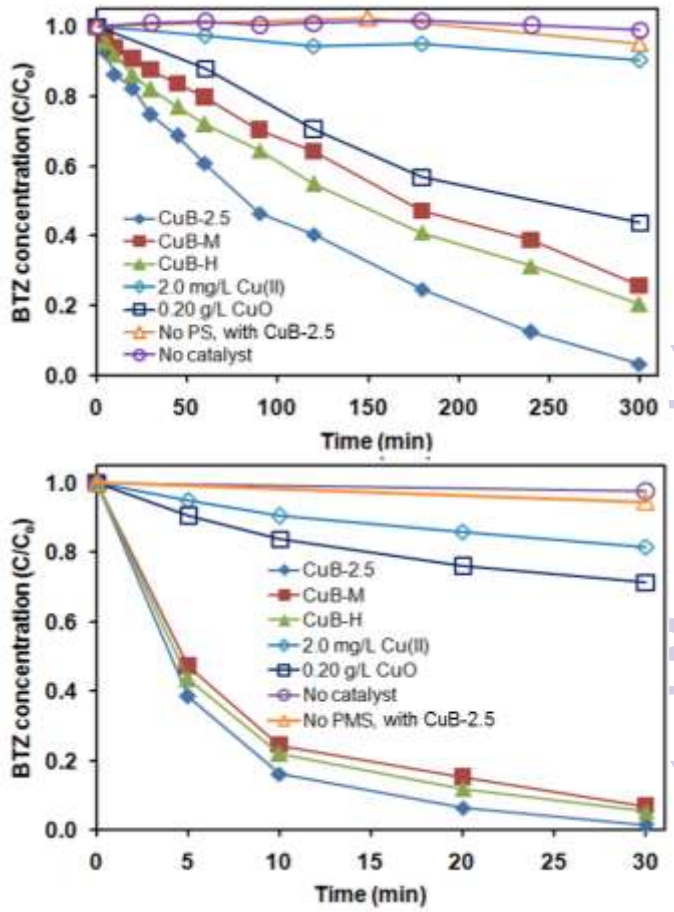

Fig. 5: BTZ removal via (a) 0.1 g L^{-1} of PS and (b) 0.05g L^{-1} of PMS activated by various catalysts. Conditions: [catalyst] = 0.5 g L^{-1}, $[BTZ]_o$ = 2.5 mg L^{-1} and $[pH]_o$ = 7.

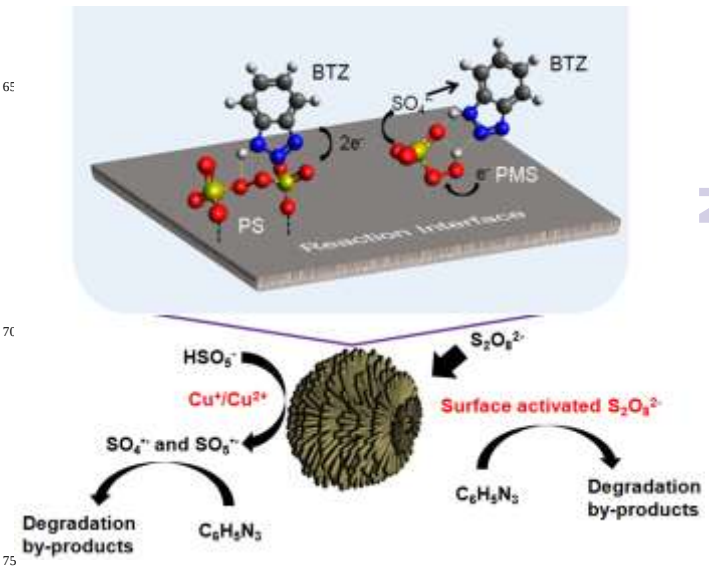

Fig. 6: Schematic illustration of the mechanisms of PS and PMS activations by CuB-2.5 for BTZ degradation.

On the other hand, the PMS activation process by CuB-2.5 is an inner sphere electron transfer reaction [5]. The PMS molecules have to be in close proximity with the catalyst for redox reaction to occur (Eqs. (6)-(8)) [31-33]. This can be easily achieved by the interaction between PMS and surface –OH group on the reaction interface. The presence of Bi^{3+} could also increase the content of –OH group in view that the pH for the isoelectric point of Bi_2O_3 is 9.4 [34]. The role of surface –OH group has been highlighted by previous researchers [35, 36]. PMS is relatively easier to be activated compared with PS possibly due to the intramolecular hydrogen bonding of the PMS molecule exposing the peroxide (-O-O-) bond for homolytic cleavage reaction (Fig. 6). The molecular structure of BTZ allows it to be drawn closer to the PMS through intermolecular hydrogen bonding which promotes BTZ oxidation within the vicinity of the catalyst. In addition, the surface –OH group can also form hydrogen bond with BTZ molecule and orientates the BTZ molecule to a planar direction favoring the attack of the electrophilic $SO_4^{\bullet-}$.

$$HSO_5^- + Cu(II) \rightarrow Cu(I) + SO_5^{\bullet-} + H^+ \quad (6)$$

$$HSO_5^- + Cu(I) \rightarrow SO_4^{\bullet-} + Cu(II) + OH^- \quad (7)$$

$$SO_4^{\bullet-} + BTZ \rightarrow \text{degradation products} \quad (8)$$

The intermolecular hydrogen bonding plays a significant role in the PS and PMS systems by (i) promoting mass transfer for BTZ degradation in the heterogeneous system, and (ii) maximizing utilization of the generated radicals. The positive role of hydrogen bond for pollutant degradation enhancement was also highlighted in other advanced oxidation systems [37]. Due to the remarkable performance of CuB-2.5, it was selected for further evaluation.

3.2.2 Parametric optimization study

3.2.2.1 PS/CuB-2.5 system

Fig. 7a-c shows the effects of different PS dosages at various catalyst loadings. The BTZ removal rate, as characterized by the initial pseudo-first order rate constant, k_1, increases linearly with increasing PS dosage and catalyst loading. However, the positive effect of increasing the PS dosage is marginal compared with increasing the catalyst loading. This provides an indirect evidence that the initial formation of the activated PS-Cu(II)Bi_2O_4 quasi-complex is an instantaneous reaction process. By limiting the reaction sites at a constant catalyst loading, rapid saturation of the reaction interface occurs immediately when PS is in contact with the catalyst and no significant change in the BTZ removal rate was observed despite further increasing the PS dosage. In this regards, the rate limiting step is the contact of BTZ with the established PS-Cu(II)Bi_2O_4 quasi-complex, which requires a specific steric orientation of the reacting functional groups to lead to the electron donation and degradation reactions. Kinetic analysis was further conducted to correlate k_1, catalyst loading and PS dosage at pH 7 using the following kinetic expression:

$$\frac{dC_t}{dt} = k_{sp}[PS]_o^m[Cat]^n C_t \quad (9)$$

where C_t is the BTZ concentration over time, k_{sp} is the specific initial rate constant and $[PS]_o$ and $[Cat]_o$ are the PS dosage and CuB-2.5 loading, respectively. By 3-D plotting of the experimentally-derived k_1 against $[Cat]_o$ and $[PS]_o$ through a forced origin intercept (Fig. 8) using MATLAB, the estimated values of m and n are 0.25 and 0.5, respectively, while the value of k_{sp} is 0.022 $g^{3/4}$ $L^{-3/4}$ min^{-1} (R^2 = 0.98). This clearly indicates that the reaction surface area is more influential than the PS dosage on BTZ removal rate by a magnitude of 2.

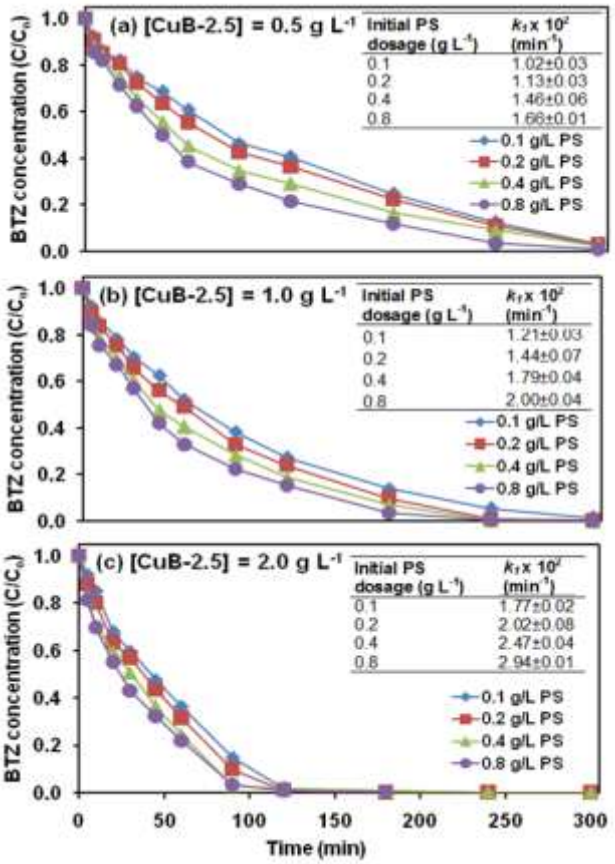

Fig. 7: BTZ removal at various initial PS dosage and (a) 0.5 g L^{-1}, (b) 1.0 g L^{-1} and (c) 2.0 g L^{-1} of CuB-2.5. Conditions: $[BTZ]_o$ = 2.5 mg L^{-1} and $[pH]_o$ = 7.

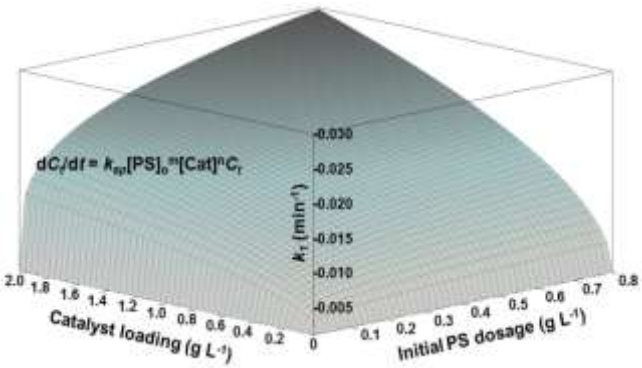

Fig. 8: Relationship between initial rate constant, initial PS dosage, and catalyst loading at pH 7.

3.2.2.2 PMS/CuB-2.5 system

Fig. 9a-c shows the effects of different initial BTZ concentrations at different PMS dosages. The trend of k_2 shows a linear increase with (i) increasing PMS dosage and (ii) decreasing initial BTZ concentration. At higher BTZ concentrations, the BTZ degradation rate is limited by the specific surface area for reaction to achieve equitable removal efficiency within the same amount of time as those at lower BTZ concentrations. The higher amount of BTZ molecule could also induce steric constraint and block the active sites of the catalyst rendering it unavailable for

PMS activation [38]. Although accumulation of the BTZ degradation by-products on the catalyst surface could also contributes to the temporal deactivation of the catalyst, it is insignificant as supported by the catalyst reusability study (Section 3.3.2). Fig. 9a also shows the remarkable effect of increasing the catalyst loading (from 0.5 to 2.0 g L^{-1}) which leads to a complete BTZ removal in less than 1 min.

3.2.3 Comparison of PS and PMS systems for BTZ degradation

3.2.3.1 Effects of Cl^-

The chloride ion is an important $SO_4^{\bullet-}$ scavenger and can react with $SO_4^{\bullet-}$ to produce $Cl^\bullet$ which will then be converted to a weaker $Cl_2^{\bullet-}$ radical (E_o = 2.09 V) [20, 39, 40] as follow:

$Cl^- + SO_4^{\bullet-} \rightarrow Cl^\bullet + SO_4^{2-}$, ($k_3 = 2.8 \times 10^8$ M^{-1} s^{-1}) (10)

$Cl^\bullet + Cl^- \rightarrow Cl_2^{\bullet-}$, ($k_4 = 8 \times 10^9$ M^{-1} s^{-1}) (11)

Fig. 10 shows the effects of Cl^- on BTZ degradation at pH 7 indicating that Cl^- exerts detrimental effects on the BTZ removal rate and efficiency in both the PS and PMS systems. In the PS system, the decrease of k_1 and BTZ removal efficiency could be attributed to two major factors, namely (i) the increase in ionic strength which is in agreement with the results reported by Zhang et al. [5] and (ii) the scavenging of miniature amount of $SO_4^{\bullet-}$ generated from the inefficient PS activation by Cu. The phenomenon (ii) plays a very minor role considering that PS activation by Cu^{2+} to generate $SO_4^{\bullet-}$ is highly inefficacious.

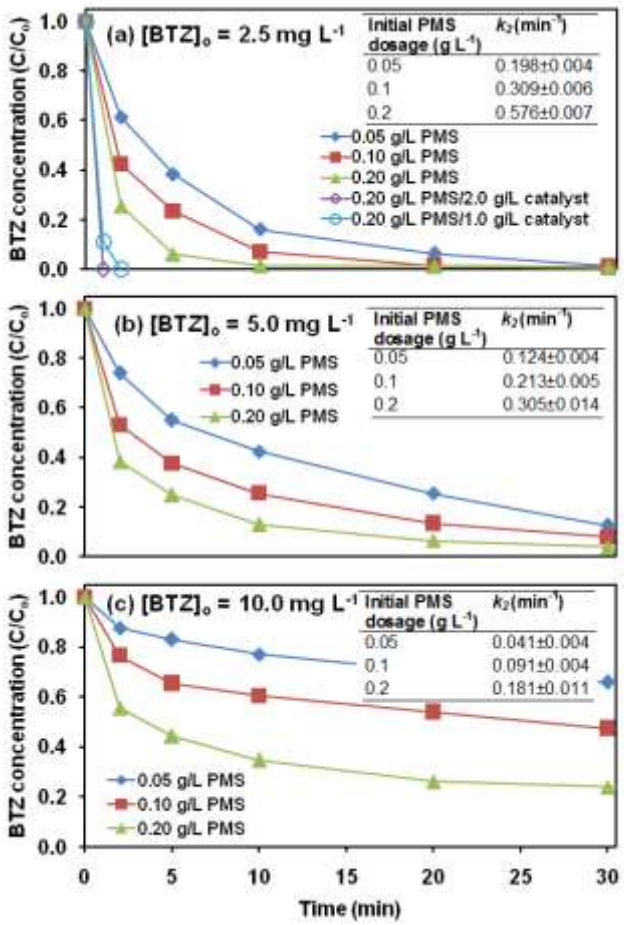

Fig. 9: BTZ removal at various initial PMS dosages and (a) 2.5 mg L^{-1}, (b) 5.0 mg L^{-1} and (c) 10.0 mg L^{-1} of BTZ. Conditions: [CuB-2.5] = 0.5 g L^{-1} and $[pH]_o$ = 7.

In the PMS system, the oxidation reaction is mainly mediated by $SO_4^{\bullet-}$ and therefore, the Cl^- ion has an adverse effect on the BTZ degradation as observed by the decrease of the k_2 value with increasing Cl^- concentration. The steady-state [$SO_4^{\bullet-}$] in the PMS reaction system was estimated from the $SO_4^{\bullet-}$ oxidation of benzene at pH 7 as follows:

Benzene + $SO_4^{\bullet-} \rightarrow$ degradation by-products + SO_4^{2-}, ($k_5 = 3 \times 10^9$ M^{-1} s^{-1}) (12)

where k_5 is the second-order rate constant for the $SO_4^{\bullet-}$+benzene reaction [24]. At pH 7, the contribution of $HO^\bullet$ in degradation of BTZ was minimal due to the slow rate of conversion of $SO_4^{\bullet-}$ to $HO^\bullet$ [39].

$SO_4^{\bullet-} + OH^- \rightarrow HO^\bullet + SO_4^{2-}$, (at pH =7, $k_6 < 60$ M^{-1} s^{-1}) (13)

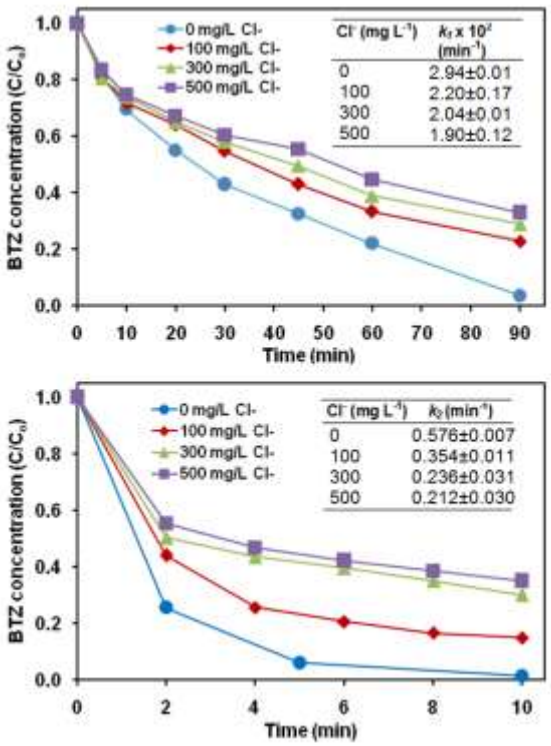

Fig. 10: Effects of Cl^- on BTZ degradation at pH 7 for (a) PS/CuB-2.5 and (b) PMS/CuB2.5 systems.

The pseudo-first order rate constant value for benzene removal in the PMS system (Fig. S3), k_7, is 0.0051±0.0004 s^{-1} and thus, the estimated steady-state [$SO_4^{\bullet-}$] is 1.7 x 10^{-12} M by calculating [$SO_4^{\bullet-}$] = k_7/k_5. In this regards, the second-order rate constant for the reaction BTZ+$SO_4^{\bullet-}$ can be estimated from the k_2 value.

$SO_4^{\bullet-}$ + BTZ → degradation by-products+ SO_4^{2-}, ($k_8 = 5.6 \times 10^9$ M^{-1} s^{-1}) (14)

This indicates that $SO_4^{\bullet-}$ reacts preferentially with BTZ than with Cl^- at the same condition. However, taking into account the high Cl^- concentration (40 times higher than BTZ), and the k_3 [Cl^-] values at 100, 300 and 500 mg L^{-1} of Cl^- are 7.9x 10^6, 2.4x 10^6, 3.9 x 10^6 s^{-1}, respectively, this indicates that the Cl^-+$SO_4^{\bullet-}$ reaction is more favorable under this condition (k_8[BTZ] = 1.2 x 10^5 s^{-1}). Nevertheless, BTZ degradation could still proceed at these Cl^- concentrations due to the production of various reactive radicals (i.e. $Cl^\bullet$, $Cl_2^{\bullet-}$ and $HO^\bullet$) from the side reactions of $Cl^\bullet$ which could also attack and degrade BTZ [41].

Table 1: Cu leaching, TOC removal, $[Oxidant]_{final}/[Oxidant]_o$, for the treatment of BTZ by the PS and PMS systems. Conditions: $[BTZ]_o$ = 2.5 mg L^{-1}, $[PS]_o$ = 0.8 g L^{-1}, $[PMS]_o$ = 0.2 g L^{-1}, t_{PS} = 90 min and t_{PMS}= 10 min.

Catalyst	[Catalyst] (g L^{-1})	Cycle	$[Oxidant]_{final}/[Oxidant]_o$	% TOC removal	Cu leaching (µg L^{-1} and %)
PS					
t_{PS} = 90 min					
Cu^{2+} (aq)	0.002	1	0.97±0.03	9	-
CuO	2.0	1	0.82±0.02	59	6561(0.04%)
CuB-M	2.0	1	0.91±0.02	18	314 (0.01%)
CuB-H	2.0	1	0.91±0.01	21	134 (<0.01%)
CuB-2.5	2.0	1	0.85±0.01	48	505 (0.02%)
	2.0	2	0.91±0.02	42	-
	2.0	3	0.91±0.03	39	-
PMS					
t_{PMS} = 10 min					
Cu^{2+}(aq)	0.002	1	0.95±0.02	8	-
CuO	0.5	1	0.87±0.03	13	2572 (0.06%)
CuB-M	0.5	1	0.80±0.02	17 (52)*	6 (<0.01%)
CuB_H	0.5	1	0.79±0.03	18 (53)*	B.D.L
CuB-2.5	0.5	1	0.78±0.01	17 (54)*	57 (<0.01%)
		2	0.82±0.01	14 (44)*	-
		3	0.83±0.02	14 (45)*	-

B.D.L. = below detection limit (0.1µg L^{-1}), (*) = % TOC removal at t = 90 min.

3.2.3.2 Cu leaching, reusability and PS/PMS consumption

The morphology of CuB-2.5 could be retained after redox reaction with PS and PMS (Fig. S4). Table 1 shows a comparison of PS and PMS systems in terms of Cu leaching and PMS/PMS_o after BTZ oxidation reaction with various catalysts. The PS/CuO indicated in Table 1 due to the inefficient PS/PMS consumption. The Cu leaching in the PMS/CuB system was at least 10 times lower than their corresponding PS/CuB system. This can be attributed to the (i) shorter treatment time (10 min vs. 90 min), and (ii) lower catalyst loading (0.5 g L^{-1} vs. 2.0 g L^{-1}). Metal dissolution especially after activation reaction is a major issue and has been heavily reported particularly for Co-based activators [32, 42].

The estimated cost of PMS required for treating 2.5 mg L^{-1} of BTZ is about 3 times more expensive than that of PS ($0.74 per kg of PS vs. $2.2 per kg of PMS) but however, the PMS/CuB-2.5 system has the potential to treat at least 8-9 times higher volume of water than PS/CuB-2.5 system. It is anticipated that the PS system could achieve the same BTZ removal rate as the PMS system by increasing the specific surface area or catalyst loading by14 times to 523.6 m^2 g^{-1} or 28 g L^{-1}, respectively. However, this is not practical since having increasing the catalyst loading could also lead to a significantly higher Cu leaching and require an additional post treatment process. In both PS/CuB-2.5 and PMS/CuB-2.5 systems, excellent reusability was observed indicating that the catalyst is stable can be consistently reused for multiple cycles with >95% BTZ removal at t = 90 min (Fig. S5).

3.2.3.3 Degradation pathways of PS/CuB-2.5 and PMS/CuB-2.5 systems

The major BTZ degradation pathways were investigated for the PS/CuB-2.5 and PMS/CuB-2.5 systems. The mass spectra (Fig. S6) after the BTZ oxidation reaction in the PS/CuB-2.5 and PMS/CuB-2.5 systems show similar profile. This indicates that the BTZ oxidation in the two systems leads to similar main oxidation intermediates (Fig. 11). In this study, two reaction intermediates, namely diazoimine (A, m/z = 106) and benzene (B, m/z = 79) are identified with the positive mode ESI. It is proposed and PMS/CuO systems showed the highest Cu leaching indicating that CuO is not suitable for PS and PMS activation processes. On the other hand, Cu^{2+} (*aq*) at 2 mg L^{-1} cannot effectively activate PS and PMS for BTZ degradation. The results commensurate with the relatively high residual PS/ PMS in the Cu^{2+} systems as that the initial oxidation of BTZ by PS and PMS could result in the generation of the several different unstable intermediates which subsequently leads to the triazole ring opening via bond scission of the N-NH. This is follow by the elimination of NH group yielding diazoimine (A, m/z 106). Similarly, Wu et al. also observed diazoimine (m/z 105) as their main BTZ oxidation intermediate in their heterogeneous photoelectro-Fenton like process [14]. Due to the instability of the diazoimine molecule, the molecule is further degraded to benzene (B) (m/z = 79) with the loss of N_2. Then, ring cleavage of the benzene ring occurs producing lower molecular weight acids and subsequently, to CO_2 and H_2O. Two peaks with higher m/z (m/z = 181 and 199) are also detected suggesting that dimerization-mineralization reaction could also occur. Dimerization-mineralization pathway is common for sulfate radical-mediated oxidation reaction [17, 43]. Besides polymerization induced by sulfate radical, BTZ polymerization to form higher molecular weight organics was also previously observed in the solar photocatalysis system [15].

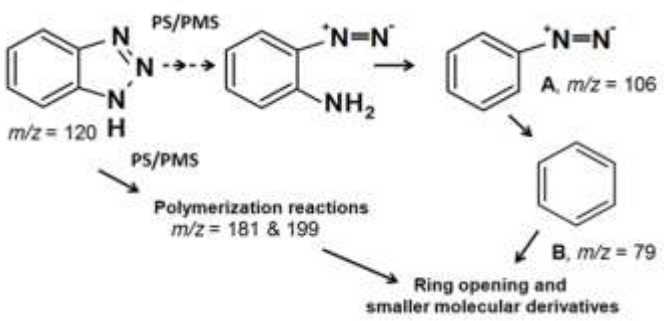

Fig. 11: Proposed major BTZ degradation pathway in the PS/CuB-2.5 and PMS/CuB-2.5 systems.

Conclusions

In this study, a novel 3-D spherical $CuBi_2O_4$ nanocolumn arrays with efficient bi-functional PS and PMS activation functionalities was successfully synthesized via a facile hydrothermal method. The catalyst (CuB-2.5) has the highest surface area and Cu content compared with other CuB catalyst (CuB-M and CuB-H) and can be employed to treat BTZ via PS and PMS activations. The CuB-2.5 catalyst performed remarkably better compared with the homogeneous Cu^{2+}, CuO, CuB-M and CuB-H. The performance of CuB-2.5 was optimized by varying the initial PMS/PS dosage, catalyst loading and initial BTZ concentration. The PMS/CuB-2.5 system was found to be more efficient than the PS/CuB-2.5 system. The inter- and intra-molecular hydrogen bonds play a crucial role in the mechanism of BTZ removal in both PS and PMS systems. The BTZ degradation pathway in the PS/CuB-2.5 and PMS/CuB-2.5 systems was similar and several intermediates were successfully identified. The CuB-2.5 catalyst could retain its morphology even after used and the reusability study indicates that it can be reused for multiple cycles. This study showed that the CuB-2.5 catalyst is a promising catalyst with bi-functional PS and PMS activation functionalities for BTZ removal.

Acknowledgement

The authors would like to thank Nanyang Environment and Water Research Institute (NEWRI) and Interdisciplinary Graduate School (IGS), Nanyang Technological University (NTU) for the award of PhD research scholarship. The kind assistances of the graduate students and staffs from the Environmental Labs and the facility for analysis characterisation testing (FACTS) are gratefully acknowledged.

Notes and references

[a]*Nanyang Environment and Water Research Institute (NEWRI), Interdisciplinary Graduate School (IGS), Nanyang Technological University, 1 Cleantech Loop, CleanTech One, Singapore 637141, Singapore.*
[b]*Division of Environmental and Water Resources Engineering, School of Civil and Environmental Engineering, Nanyang Technological University, 50 Nanyang Avenue, Singapore 639798, Singapore.*
[c]*School of Materials Science and Engineering, Nanyang Technological University, 50 Nanyang Avenue, Singapore 639798, Singapore.*
*Corresponding author. Tel: +65-6790 6933, Fax: +65-6791 0676, *E-mail address:* cttlim@ntu.edu.sg (Lim T.T.)
† Electronic Supplementary Information (ESI) available: [details of any supplementary information available should be included here]. See DOI: 10.1039/b000000x/

References

[1] P. Shukla, I. Fatimah, S. Wang, H.M. Ang, M.O. Tadé, Catalysis Today 157 (2010) 410-414.
[2] S. Yang, P. Wang, X. Yang, L. Shan, W. Zhang, X. Shao, R. Niu, Journal of Hazardous Materials 179 (2010) 552-558.
[3] T. Olmez-Hanci, C. Imren, I. Kabdasl, O. Tunay, I. Arslan-Alaton, Photochemical & Photobiological Sciences 10 (2011) 408-413.
[4] H. Sun, X. Feng, S. Wang, H.M. Ang, M.O. Tadé, Chemical Engineering Journal 170 (2011) 270-277.
[5] T. Zhang, Y. Chen, Y. Wang, J. Le Roux, Y. Yang, J.-P. Croué, Environmental Science & Technology 48 (2014) 5868-5875.
[6] F. Ji, C. Li, L. Deng, Chemical Engineering Journal 178 (2011) 239-243.
[7] W.-D. Oh, S.-K. Lua, Z. Dong, T.-T. Lim, Journal of Hazardous Materials 284 (2015) 1-9.
[8] V. Matamoros, E. Jover, J.M. Bayona, Occurrence and fate of benzothiazoles and benzotriazoles in constructed wetlands, Water Science and Technology, 2010, pp. 191-198.
[9] X. Liang, M. Wang, X. Chen, J. Zha, H. Chen, L. Zhu, Z. Wang, Chemosphere 112 (2014) 154-162.
[10] I. Briguglio, S. Piras, P. Corona, E. Gavini, M. Nieddu, G. Boatto, A. Carta, European Journal of Medicinal Chemistry.
[11] H.-G. Ni, F.-H. Lu, X.-L. Luo, H.-Y. Tian, E.Y. Zeng, Environmental Science & Technology 42 (2008) 1892-1897.
[12] D. Voutsa, P. Hartmann, C. Schaffner, W. Giger, Environ Sci Pollut Res 13 (2006) 333-341.
[13] N.K. Vel Leitner, B. Roshani, Water Research 44 (2010) 2058-2066.
[14] J. Wu, W. Pu, C. Yang, M. Zhang, J. Zhang, Journal of Environmental Sciences 25 (2013) 801-807.
[15] J. Xu, L. Li, C. Guo, Y. Zhang, S. Wang, Chemical Engineering Journal 221 (2013) 230-237.
[16] A.S. Ruhl, F. Zietzschmann, I. Hilbrandt, F. Meinel, J. Altmann, A. Sperlich, M. Jekel, Chemical Engineering Journal 257 (2014) 184-190.
[17] W.-D. Oh, S.-K. Lua, Z. Dong, T.-T. Lim, Journal of Materials Chemistry A 2 (2014) 15836-15845.
[18] H. Sun, C. Kwan, A. Suvorova, H.M. Ang, M.O. Tadé, S. Wang, Applied Catalysis B: Environmental 154–155 (2014) 134-141.
[19] G.P. Anipsitakis, D.D. Dionysiou, Environmental Science & Technology 37 (2003) 4790-4797.
[20] S. Padmaja, P. Neta, R.E. Huie, International Journal of Chemical Kinetics 25 (1993) 445-455.
[21] G.P. Anipsitakis, D.D. Dionysiou, M.A. Gonzalez, Environmental Science & Technology 40 (2005) 1000-1007.
[22] H.V. Lutze, N. Kerlin, T.C. Schmidt, Water Research.
[23] A.M. Abdulkarem, J. Li, A.A. Aref, L. Ren, E.M. Elssfah, H. Wang, Y. Ge, Y. Yu, Materials Research Bulletin 46 (2011) 1443-1450.
[24] P. Neta, V. Madhavan, H. Zemel, R.W. Fessenden, Journal of the American Chemical Society 99 (1977) 163-164.
[25] F.P. Tully, A.R. Ravishankara, R.L. Thompson, J.M. Nicovich, R.C. Shah, N.M. Kreutter, P.H. Wine, The Journal of Physical Chemistry 85 (1981) 2262-2269.
[26] C.S. Liu, K. Shih, C.X. Sun, F. Wang, Science of The Total Environment 416 (2012) 507-512.
[27] M. Faisal, S.B. Khan, M.M. Rahman, A. Jamal, A. Umar, Materials Letters 65 (2011) 1400-1403.
[28] Y. Bo, B. Huang, Y. Zhang, J. Wang, W.M. Lau, Z. Zheng, Powder Technology 264 (2014) 396-400.
[29] S.P. Berglund, H.C. Lee, P.D. Nunez, A.J. Bard, C.B. Mullins, Physical Chemistry Chemical Physics 15 (2013) 4554-4565.
[30] A. Klinbumrung, T. Thongtem, S. Thongtem, Applied Surface Science 313 (2014) 640-646.
[31] G.P. Anipsitakis, D.D. Dionysiou, Environmental Science & Technology 38 (2004) 3705-3712.
[32] G.P. Anipsitakis, E. Stathatos, D.D. Dionysiou, The Journal of Physical Chemistry B 109 (2005) 13052-13055.

[33] T. Zhang, H. Zhu, J.-P. Croué, Environmental Science & Technology 47 (2013) 2784-2791.
[34] M. Kosmulski, Advances in Colloid and Interface Science 152 (2009) 14-25.
[35] W. Zhang, H.L. Tay, S.S. Lim, Y. Wang, Z. Zhong, R. Xu, Applied Catalysis B: Environmental 95 (2010) 93-99.
[36] Y. Ren, L. Lin, J. Ma, J. Yang, J. Feng, Z. Fan, Applied Catalysis B: Environmental 165 (2015) 572-578.
[37] R. Vargas, O. Núñez, Journal of Molecular Catalysis A: Chemical 300 (2009) 65-71.
[38] F. Ji, C. Li, Y. Liu, P. Liu, Separation and Purification Technology 135 (2014) 1-6.
[39] P. Neta, R.E. Huie, A.B. Ross, Journal of Physical and Chemical Reference Data 17 (1988) 1027-1284.
[40] V. Nagarajan, R.W. Fessenden, The Journal of Physical Chemistry 89 (1985) 2330-2335.
[41] G.-D. Fang, D.D. Dionysiou, Y. Wang, S.R. Al-Abed, D.-M. Zhou, Journal of Hazardous Materials 227–228 (2012) 394-401.
[42] R. Patil, S. Kelkar, R. Naphade, S. Ogale, Journal of Materials Chemistry A 2 (2014) 3661-3668.
[43] T.K. Lau, W. Chu, N.J.D. Graham, Environmental Science & Technology 41 (2006) 613-619.